Entanglement Dynamics and Chaos in the Dicke Model

**Lijun Song · Xiaoguang Wang · Dong Yan ·
ZhanGuo Zong**

Abstract We study dynamical properties of quantum entanglement in the Dicke model with
and without the rotating-wave approximation. Specifically, we investigate the maximal en-
tanglement and mean entanglement which reflect the underlying chaos in the system, and
a good classical-quantum correspondence is found. We also show that the maximal linear
entropy can be more sensitive to chaos than the mean linear entropy.

Keywords Entanglement · Chaos · Linear entropy

1 Introduction

Entanglement plays a key role in the rapidly developing field of quantum information
processing. It has been recognized as a quantum resource for information processing such as
quantum teleportation [1], quantum cryptography [2], and quantum dense coding [3–5]. Al-
though the definition of entanglement itself is not of dynamical nature, entangled states are
often generated dynamically. To understand the entanglement process, it is of importance to
study simple Hamiltonian systems, in particular the nonlinear systems.

Hamiltonian systems with two degrees of freedom often present a very rich dynamics,
which in many cases are not yet completely understood from a general point of view. If the

L. Song · Z. Zong
Institute of Applied Physics, Changchun University, Changchun 130022, P.R. China

L. Song · D. Yan
School of Science, Changchun University of Science and Technology, Changchun 130022, P.R. China

L. Song · X. Wang
Zhejiang Institute of Modern Physics, Department of Physics, Zhejiang University, HangZhou 310027,
P.R. China

D. Yan (✉)
School of Science, Lanzhou University of Technology, Lanzhou 730050, P.R. China
e-mail: ydbest@126.com

interaction is nonlinear the system may present chaotic behavior in the classical limit. The consequences of this fact to the quantum dynamics is yet an unsettled issue. A step in this direction was taken a few years ago, as it was believed that the rate of entropy production can be used as an intrinsically quantum test of the chaotic versus regular nature of the evolution [17, 18]. In general, chaotic systems tend to produce larger entanglement than the regular systems. However, exceptions for a system with classically regular behaviors are found in Refs. [19, 20].

Recently, the Dicke model has been extensively studied in the literature [10–14, 21–25]. Here, we consider the dynamical properties of entanglement of atoms and field with and without the rotating wave approximation (RWA). Specifically, the mean and maximal entanglement are studied to reveal the underlying chaos in the system. The linear entropy, decoherence, concurrence [6, 7] and spin squeezing [7–9, 15, 16] can be exploited to study quantum entanglement. Here, we use linear entropy to quantify entanglement.

The paper is organized as follows. In Sect. 2, we introduce the classical analog of the Dicke model and define some quantities such as the line entropy, the maximal entanglement and the mean entanglement. In Sect. 3, we discuss the dynamics behaviors of classical chaos and quantum entanglement, and the relations between them. Conclusions are given in Sect. 4.

2 The Dicke Model and the Linear Entropy

We consider a generalized version of N-atom Dicke model that describes a collection of N two-level atoms interacting with a single-mode radiation field. Moreover, since our aim here is to pursue the effect of the classically chaos on the entanglement between the atoms and the field, we will ignore the interaction between the atoms (qubits) and treat the atom system as a large spin ($N = 2J$) ($\hbar = 1$ hereafter)

$$H = \omega J_z + \omega_0 a^\dagger a + \frac{R}{\sqrt{2J}} \left(J_+ a + J_- a^\dagger \right)$$

$$+ \frac{R'}{\sqrt{2J}} \left(J_+ a^\dagger + J_- a \right). \tag{1}$$

Here, ω and ω_0 are frequencies associated with free Hamiltonians for atoms and field, respectively. R, R' are coupling parameters. The usual RWA is recovered by setting $R' = 0$. The field observable are described by means of the creation and annihilation operators a and $a^\dagger$, whereas J_z, $J_\pm$ are the collective atomic pseudospin operators. These operators satisfy the following commutation relations,

$$[a, a^\dagger] = 1, \tag{2}$$

$$[J_z, J_\pm] = \pm J_\pm. \tag{3}$$

This model is used to describe both, cavity QED experiments [26, 27] and trapped-ion systems. In the last system, interactions with different couplings $R \neq R'$ can be generated [28, 29].

In our case, we take the initial states to be coherent states (CS), namely, minimum uncertainty wave packets centered in the corresponding classical phase spaces. That allows us

to explore the relation between the entanglement and classical chaos. The initial quantum states chosen in the present study are as follows,

$$|\psi(0)\rangle = |\mu\rangle \otimes |\nu\rangle \equiv |\mu\nu\rangle, \tag{4}$$

where, the appropriate initial state $|\mu\nu\rangle$ is a product of the atomic and field CS defined as [30–32]:

$$|\mu\rangle = (1 + \mu\mu^*)^{-j} e^{\mu J_+} |j, -j\rangle, \tag{5}$$

$$|\nu\rangle = e^{-\nu\nu^*/2} e^{\nu a^\dagger} |0\rangle. \tag{6}$$

Here, $J = N/2$ and the variables μ and ν can be written as a function of the classical variables in the corresponding phase spaces, (q_1, p_1) for the atomic degree of freedom, and (q_2, p_2) for the field

$$\mu = \frac{q_1 + ip_1}{\sqrt{4J - (q_1^2 + p_1^2)}}, \tag{7}$$

$$\nu = \frac{1}{\sqrt{2}}(q_2 + ip_2). \tag{8}$$

A corresponding classical Hamiltonian can been obtained by a standard procedure [33], using the above defined CS $\langle\mu\nu| H |\mu\nu\rangle$ [34, 35]

$$\mathcal{H}(q_1, p_1, q_2, p_2) = \frac{\omega}{2}\left(p_1^2 + q_1^2 - 2J\right) + \frac{\omega_0}{2}\left(p_2^2 + q_2^2\right)$$
$$+ \frac{\sqrt{4J - (p_1^2 + q_1^2)}}{4J}\left(R_- p_1 p_2 + R_+ q_1 q_2\right) \tag{9}$$

with $R_\pm = R \pm R'$.

To study dynamics of entanglement, one must choose an entanglement measure. These measures include entanglement of formation [4], linear entropy [5], entanglement of distillation [36], concurrence [37], relative entropy of entanglement [38, 39], negativity [40], and so on. In our cases, the entanglement can be described by the linear entropy or the von Neumann entropy. We calculate the linear entropy and the von Neumann entropy, respectively, and the similar behavior of the two measures is found. Thus we only present the results of the linear entropy.

The linear entropy is defined as [4]

$$E_l(t) = 1 - \mathrm{Tr}_1 \rho_1(t)^2, \tag{10}$$

where Tr_1 denote a trace over the first subsystem, and $\rho_1(t)$ is the reduced-density matrix, $\rho_1(t) = \mathrm{Tr}_2 |\psi(t)\rangle\langle\psi(t)|$, where indices 1 and 2 stand for atoms and field subsystem, respectively, and $|\psi(t)\rangle$ is the quantum state of the full system, which evolves in time under the action of Hamiltonian (1). In this study, we also explore both the maximal entanglement and mean entanglement over all time. In practice, for numerical purposes we consider a finite time domain. We define maximal entanglement $E_{\max}$ and mean entanglement E_{mean} as follows

$$E_{\max} = \max_t \{E_l(t)\},$$

$$E_{\text{mean}} = \frac{1}{T} \int_0^T E_l(t), \tag{11}$$

where T is cut off time. Now, we start to explore the behaviors of entanglement dynamics.
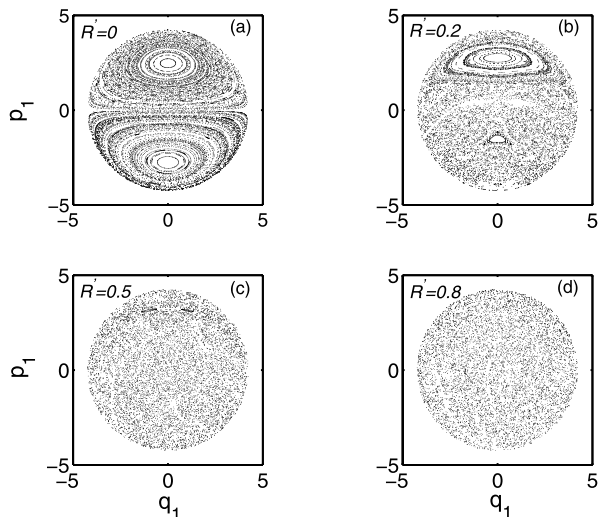
3 The Entanglement Dynamics

We will discuss (i) the dynamics behaviors of classical chaotics, (ii) the relation between the entanglement and coupling parameters, (iii) the effects of the initial conditions on the entanglement, and (iv) the influence of dimension of atomic system on the entanglement.

3.1 The Dynamics Behaviors of Classical Chaotics

The classical dynamics associated with this Hamiltonian were explored before [34, 35]. It is shown that the integrable situations are recovered when either R or R' is zero, and the most chaotic dynamics is associated with the condition $R = R'$. Our aim is to investigate the time evolution of the initially quasi-classical wave-packet along with the occurrence of entanglement between the atom and the field systems. Particularly, we are looking for the possible differences in the wave-packet dynamics when we compare *integrable* and *non-integrable* interactions. The connection with the classical dynamics is established by choosing CS as initial states, centered at the corresponding points of the phase space. Then, we let the system evolve by means of the Hamiltonian (1) and explore the entanglement dynamics solving numerically the Schrödinger equation. In Fig. 1 we show the Poincaré section of the classical counterpart for the spin degree of freedom, defined by the section $q_2 = 0$ in the four-dimensional phase space so that every time a trajectory pierces this section with $p_2 > 0$ the corresponding point (q_1, p_1) is plotted. The surfaces of section correspond to the Fig. 1, the first one [Fig. 1a] is the integrable case ($R' = 0$) and the second one [Fig. 1b]

Fig. 1 Poincaré sections for the classical Dicke model for four coupling parameters, $R' = 0, 0.2, 0.5, 0.8$ ($R = 0.5$), with $N = 9$ and $E = 8.5$

is the soft chaos ($R' = 0.2$). Another two figures [Fig. 1c, Fig. 1d] correspond the stronger chaos ($R' = 0.5$) and ($R' = 0.8$), respectively. Here, the total energy is fixed at $E = 8.5$, $J = 4.5, \omega = \omega_0 = 1$. The limit of atomic phase space is indicated by a border at radius equal to $\sqrt{4J}$. Integrable section shows a separatrix of motion along the line $p_1 = 0.0$ and concentric tori around each of the two stable periodic orbits in Fig. 1a. A pro-eminent feature of the non-integrable surface of section is a large stability island for $p_1 > 0$ and a small stability island for $p_1 < 0$ in Fig. 1b.

3.2 The Effects of the Initial Conditions on the Entanglement

Now, we start from studying dynamics behaviors of entanglement for initial coherent states with a mean value centered in the different regions of the phase space. We choose the line ($q_1 = 0$), which includes all the different regions we are exploring. For the integrable case as in Fig. 1a, we choose two fixed points at $p_1 = 2.52$ and $p_1 = -2.87$, which is in the internal tori belonging to this region, and another $p_1 = 0$ located at a boundary. For the non-integrable case as in Fig. 1b, we choose a fixed point $p_1 = 2.85$ which is in the stability island, $p_1 = 1.82$ corresponding to a regular and chaos border, and a point $p_1 = 0.8$ is well in the chaotic sea.

Figures 2 and 3 shows the numerical results of the linear entropy E_L. For the integrable case (see Fig. 2). The entanglement for the state initially centered at stable fixed point displays smaller increases, but at the boundary ($p_1 = 0$) it reveals a comparatively much faster increase. This can be viewed as the so-called border effect [43]. At the boundary, more disorders are involved, and this leads to large entropy production. For the non-integrable case (see Fig. 3), the entanglement for the state initially centered at stability island fixed point displays a clear single frequency at short time. We observe that entanglement have a rapid rise after a very short time for the initial state centered in the chaotic region. As the dynamics evolves, then the entropy saturate to a relatively stable value for a state centered in the chaotic region. The curve with $p_1 = 0.8$ displays the intermediate behaviors.

In Fig. 4, we plot the long-time behaviors of the linear entropy for $p_1 = 0$. We observe strong oscillations of entanglement, which results from the chosen initial state well located at a chaotic region. Indeed, we see that there is a good quantum-classical correspondence,

Fig. 2 Dynamical evolution of linear entropy for the initial CS with $q_1 = 0$ and different p_1. This corresponds to the integrable case as in Fig. 1a. The parameter $N = 9$
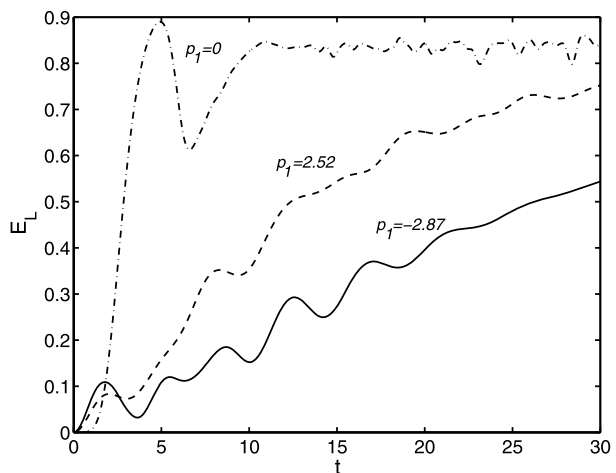
Fig. 3 Dynamical evolution of linear entropy for the initial CS with $q_1 = 0$ and different p_1. This corresponds to the non-integrable cases in Fig. 1b. The parameter $N = 9$
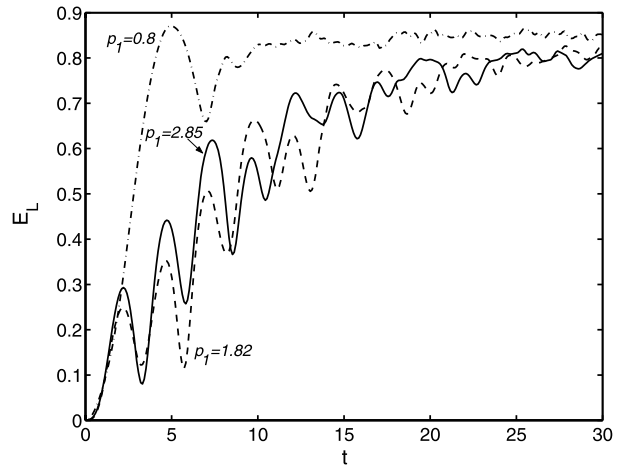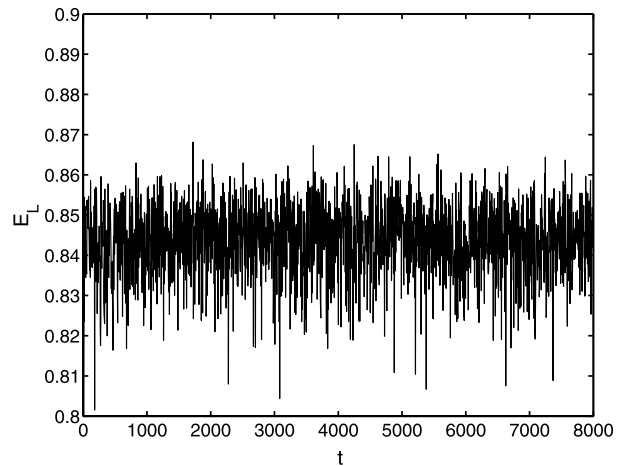

Fig. 4 Long-time behavior of the linear entropy for $q_1 = 0$ and $p_1 = 0.8$ as in Fig. 1b. The average is over 8000 steps. The parameter $N = 9$

namely, the underlying classical chaos have a strong effects on the quantum behaviors of entanglement. Conversely, we can know the underlying classical chaos by studying the quantum entanglement.

3.3 The Maximal and Mean Entanglement

To further study the quantum-classical correspondence, we now consider the maximal and mean entropy. The maximal entanglement E_{max} and mean entanglement E_{mean} here can be considered as entangling powers of our unitary operations, describing the capability of entropy production. For comparison, we take the CS constructed from the points in the straight line at $q_1 = 0$ at the four sections (Fig. 1). Thus the initial states are only determined by the values of p_1. Figure 5 displays the mean and maximal linear entropy as a function of the p_1. For the integrable case [Fig. 1a], when q_1 goes from -4 to the first stable periodic orbits, the mean linear entropy decreases until it reaches minimum which approximately corresponds to the fixed point at $p_1 = -2.87$. Subsequently, the mean linear entropy increases to a flat region. Then, the mean linear entropy decreases again due to the approaching to another

Fig. 5 Maximal linear entropy and mean linear entropy against p_1, corresponding to the straight line at $q_1 = 0$ in Poincaré sections in Fig. 1. The parameters $N = 9$
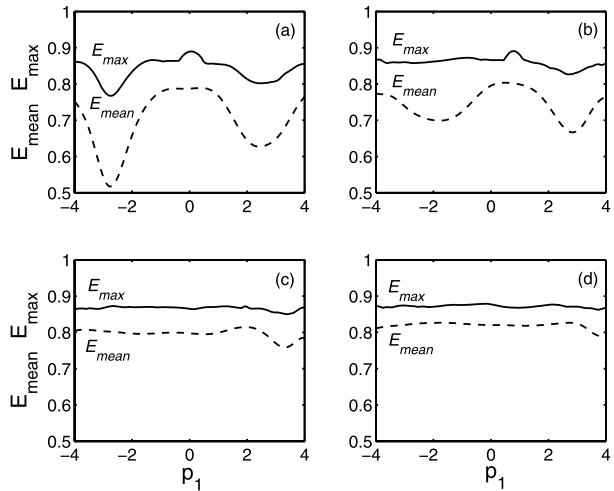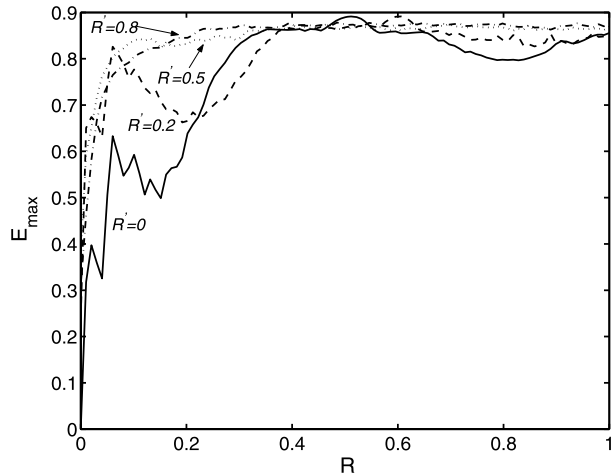

Fig. 6 Maximal linear entropy against coupling parameters R. The curves from bottom to top are for $R' = 0, 0.2, 0.5, 0.8$. The average is over 30 steps. The parameters $N = 9$

fixed point at $p_1 = -2.52$. It is very clear that the two dips of the entropy corresponds to the two classical fixed points, and the system produce smaller entanglement.

For the non-integrable case [Fig. 5b] with weak coupling ($R' = 0.2$), the two dips of the entropy correspond to the two classical fixed points at $p_1 = -1.5$ and $p_1 = 2.85$. For the strong coupling [Fig. 1c and Fig. 1d], the mean entanglement also fluctuates with p_1 with the smaller amplitude. We see that the mean entanglement displays clearly the quantum-classical correspondence. Minimum values of entropy correspond to the fixed points, and large entanglement area to the chaotic region.

The maximal linear entropy displays similar behaviors to the mean linear entropy. However, we find that the curves have displays a clear convex area for the integrable case at $p_1 = 0$ [see Fig. 5a] and the non-integrable case at $p_1 = 0.8$ [see Fig. 5b]. This means that the maximal linear entropy is more sensitive to chaos than the mean linear entropy.

Figure 6 shows the maximal entanglement versus coupling parameter R for different R'. For the integrable case, the maximal entanglement begins from zero, while for the non-integrable case, initially, the maximal entanglement is not zero. For the integrable case

Fig. 7 The dependence of the maximal linear entropy versus N and R. The parameters $q_1 = 0$, $R' = 0$, corresponding to the integrable cases in Fig. 1a
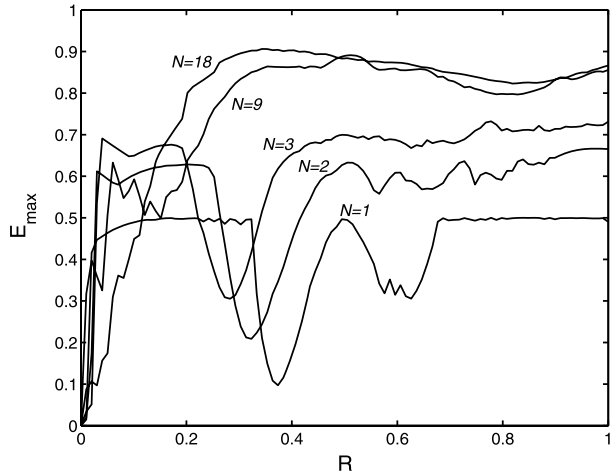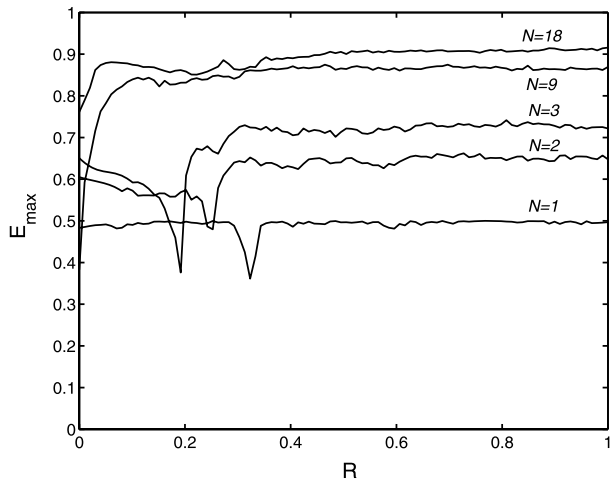

Fig. 8 Maximal linear entropy versus N and R. The parameters $q_1 = 0$, $R' = 0.5$, corresponding to the non-integrable cases as in Fig. 1c

($R' = 0$) and the case of soft chaos ($R' = 0.2$), we observe that the maximal entanglement has a strong oscillation with the increase of the coupling parameter R. For the stronger chaos ($R' = 0.5$) and ($R' = 0.8$), the maximal entanglement exhibits a rapid rise with R, then saturate to a steady value. Weak oscillations appears in these cases. Similar behaviors also appears in the coupled standard maps [41, 42].

3.4 The Influence of the Dimension on the Entanglement

In this subsection, we pay more attention to the effects of dimension on the entanglement. Here, we consider how the maximal linear entropy varies with the number of atoms N. The numerical results are given in Figs. 7 and 8. The curves from bottom to top are for $N = 1$, 2, 3, 9, and 18. We found that there are similar behaviors of the maximal entanglement when we vary N for the both the integrable and non-integrable cases. On average, the maximal entanglement E_{max} increases as N increases. For the small number of atoms, E_{max} first displays a rapid rise with R, then shows some oscillations until it reaches a stable value.

For larger number of atoms, $E_{\max}$ rapidly reaches a maximal value with weak oscillations. For the non-integrable case, initially, the $E_{\max}$ is not zero. The maximal entanglement $E_{\max}$ also have weak oscillations for the small the number of atoms. It is shown that the maximal entanglement is more sensitive to R for the small number of atoms.

4 Conclusion

In conclusion, we have studied the dynamical properties of entanglement in the Dicke model for both the integrable and non-integrable cases. The dynamics of the linear entropy are found to be strongly dependent on the initial CS. The entanglement displays a rapid rise after a very short time for an initial CS centered in a chaotic region of the phase space, whereas the entanglement displays a single frequency for the CS centered in the fixed point. The mean and maximal linear entropy over time have been used to study quantum-classical correspondence. It is shown the maximal linear entropy is more sensitive to chaos than the mean linear entropy. A very good quantum-classical correspondence was found in the behaviors of maximal and mean entanglement. We also studied the effects of dimension on entanglement. It is desirable to study entanglement in other models of quantum chaos with similar tools used here, and investigate the universality of the entanglement features.

References

1. Bennett, C.H., Brassard, G., Crepeau, C., Josza, R., Peres, A., Wootters, W.K.: Phys. Rev. Lett. **70**, 1895 (1993)
2. Nielsen, M.A., Chuang, I.L.: Quantum Computation and Quantum Information. Cambridge University Press, Cambridge (2000)
3. Bennett, C.H., Wiesner, S.J.: Phys. Rev. Lett. **69**, 2881 (1992)
4. Bennett, C.H., Bernstein, H.J., Popescu, S., Schumacher, B.: Phys. Rev. A **53**, 2046 (1996)
5. Bennett, C.H., DiVincenzo, D.P., Smolin, J.A., Wootter, W.K.: Phys. Rev. A **54**, 3824 (1996)
6. Wootters, W.K.: Phys. Rev. Lett. **80**, 2245 (1998)
7. Wang, X., Sanders, B.C.: Phys. Rev. A **68**, 012101 (2003)
8. Sørensen, A., Duan, L.M., Cirac, I., Zoller, P.: Nature **63**, 409 (2001)
9. Ulam-Orgikh, D., Kitagawa, M.: Phys. Rev. A **64**, 052106 (2001)
10. Angelo, R.M., Furuya, K.: Phys. Rev. A **71**, 042321 (2005)
11. Hou, X.W., Chen, J.H., Hu, B.: Phys. Rev. A **71**, 034302 (2005)
12. Angelo, R.M., et al.: Physica A **338**, 458 (2004)
13. Emary, C., Brandes, T.: Phys. Rev. Lett. **90**, 044101 (2003)
14. Emary, C., Brandes, T.: Phys. Rev. A **69**, 053804 (2004)
15. Yan, D., Wang, X., Wu, L.A.: Chin. Phys. Lett. **22**, 271 (2005)
16. Song, L.J., Wang, X., Yan, D., Zong, Z.G.: J. Phys. B: At. Mol. Opt. Phys. **39**, 559 (2006)
17. Zurek, W.H., Paz, J.P.: Physica D **83**, 300 (1995)
18. Zurek, W.H., Habib, S., Paz, J.P.: Phys. Rev. Lett. **70**, 1187 (1993)
19. Tanaka, A.: J. Phys. A **29**, 5475 (1996)
20. Angelo, R.M., Furuyu, K., Nemes, M.C., Pellegrino, G.Q.: Phys. Rev. E **60**, 5407 (1999)
21. Milonni, P.W., Ackerhalt, J.R., Galbraith, H.W.: Phys. Rev. Lett. **50**, 966 (1983)
22. Milonni, P.W., Shih, M.L., Ackerhalt, J.R.: Chaos in Laser-Matter Interactions. World Scientific Lecture Notes in Physics, vol. 6. World Scientific, Singapore (1987)
23. Finney, G.A., Gea-Banacloche, J.: Phys. Rev. E **54**, 1449 (1996)
24. Furuya, K., Nemes, M.C., Pellegrino, G.Q.: Phys. Rev. Lett. **80**, 5524 (1998)
25. Sanz, L., Furuya, K.: quant-ph/0507025 (2005)

26. Solano, E., Agarwal, G.S., Walther, H.: Phys. Rev. Lett. **90**, 027903 (2003)
27. Davidovich, L., Maali, A., Brune, M., Raimond, J.M., Haroche, S.: Phys. Rev. Lett. **71**, 2360 (1993)
28. Cirac, J.I., Parkins, A.S., Blatt, R., Zoller, P.: Adv. At. Mol. Opt. Phys. **37**, 237 (1996)
29. Solano, E., de Matos Filho, R.L., Zagury, N.: Phys. Rev. Lett. **87**, 060402 (2001)
30. Arecchi, F.T., Courtens, E., Gilmore, R., Thomas, H.: Phys. Rev. A **6**, 2211 (1972)
31. Glauber, R.J.: Phys. Rev. **131**, 2766 (1963)
32. Zhang, W.M., Feng, D.H., Gilmore, R.: Rev. Mod. Phys. **62**, 867 (1990)
33. Kramer, P., Saraceno, M.: Geometry of the Time-Dependent Variational Principle in Quantum Mechanics. Lecture Notes in Physics, vol. 140. Springer, New York (1981)
34. de Aguiar, M.A.M., Furuya, K., Lewenkopf, C.H., Nemes, M.C.: Ann. Phys. **216**, 291 (1992)
35. de Aguiar, M.A.M., Furuya, K., Lewenkopf, C.H., Nemes, M.C.: Europhys. Lett. **15**, 125 (1991)
36. Bennett, C.H., Brassard, G., Popescu, S., Schumacher, B., Smolin, J., Wootters, W.K.: Phys. Rev. Lett. **76**, 722 (1996)
37. Hill, S., Wootters, W.K.: Phys. Rev. Lett. **78**, 5022 (1997)
38. Vedral, V., Plenio, M.B., Jacobs, K., Knight, P.L.: Phys. Rev. A **56**, 4452 (1997)
39. Vedral, V., Plenio, M.B., Rippin, M.A., Knight, P.L.: Phys. Rev. Lett. **78**, 2275 (1997)
40. Zyczkowski, K., Horodecki, P., Sanpera, A., Lewenstein, M.: Phys. Rev. A **58**, 883 (1998)
41. Lakshminarayan, A.: Phys. Rev. E **64**, 036207 (2001)
42. Hou, X., Hu, B.: Phys. Rev. A **69**, 042110 (2004)
43. Anglo, R.M., Furuya, K., Nemes, M.C., Pellegrino, G.Q.: Phys. Rev. E **60**, 5407 (1999)